

# Axial Strain Imaging Using a Local Estimation of the Scaling Factor from RF Ultrasound Signals

ELISABETH BRUSSEAU,<sup>1</sup> CHRISTIAN PERREY,<sup>2</sup> PHILIPPE DELACHARTRE,<sup>1</sup> MICHAEL VOGT,<sup>2</sup>  
DIDIER VRAY<sup>1</sup> AND HELMUT ERMERT<sup>2</sup>

<sup>1</sup> *CREATIS*  
CNRS Research Unit (UMR 5515)  
affiliated to INSERM  
Lyon, France  
brusseau@creatis.insa-lyon.fr

<sup>2</sup> *Department of Electrical Engineering*  
Ruhr-University  
D-44780 Bochum, Germany

The main signal-processing techniques used in elastography compute strains as the displacement derivative. They perform well for very low deformations, but suffer rapidly from decorrelation noise. Aiming to increase the range of accurate strain measurements, we developed an adaptive method based on the estimation of strains as local scaling factors. Its adaptability makes this method appropriate for computing scaling factors resulting from larger strains or a wide spread of strain variations. First, segments corresponding to the same part of tissue are adaptively selected in the rest and stressed state echo signals. Then, local scaling factors are estimated by iteratively varying their values until reaching the zero of the phase of the complex cross-correlation function.

Results from simulation and from experimental data are presented. They show how this adaptive method can track various local deformations and its accuracy for strain up to 7%.

**KEY WORDS:** Adaptive estimation; complex cross-correlation; elastography; phase; scaling factor; strain; ultrasound.

## 1. INTRODUCTION

Determining the elastic properties of soft biological tissues is of fundamental interest in clinical diagnosis because of the correlation between the healthy or pathological state of a tissue and its stiffness. Indeed, many cancers, such as breast carcinomas, are characterized by the presence of extremely hard nodules, resulting from a higher stromal density.<sup>1</sup> Identically, the atherosclerosis, which consists in a focal accumulation of fatty, fibrous and blood deposits, results in a modification of the elasticity of blood-vessel walls. Over the last few years, it was shown that ultrasound is able to detect the spatial variations in the elastic properties of biological tissue. This has led to a new imaging technique, termed elastography, which visualizes the deformation behavior of a tissue in response to an externally applied mechanical compression. In practical terms, ultrasonic rf signals are acquired from a tissue in both rest and stressed states. Maps of local strains are then generated by evaluating the variations within the signals induced by the stress.

It is essential to estimate strains with high accuracy in elastography, since clinicians' diagnoses will be directly related to those estimations. This requires a processing, that fits the local variations of the strain. Let us consider a medium composed of layers of low Young's moduli or of Young's moduli of several magnitudes difference. Under compression, this medium will be exposed to large deformations or to large discontinuities in the strain pat-

tern.<sup>2</sup> Since a significant dynamic range of strains is expected in biological tissues, computing the strain profile requires an algorithm with locally-adaptive parameters, like the displacement of the window of study.

So far, the most common signal-processing techniques used in elastography are gradient-based methods, which estimate strain as the displacement derivative. In the case of small deformations, the ultrasonic signal acquired after compression is assumed to be a delayed replica of the precompression signal. The local tissue displacement is, in this case, a simple shift. It is computed as the location of the maximum of the cross-correlation function of gated pre- and postcompression echo signals,<sup>1,3-7</sup> or as the zero of the phase of the complex correlation function of the corresponding baseband signals.<sup>8-11</sup> Although this technique performs well for very small deformations (0.25%-1%), it fails rapidly with increasing strain. The explanation is simple: with the physical compression of the tissue, the signal is subjected to a variation in shape which is responsible for the decorrelation noise. One possible improvement is to stretch the postcompression signal temporally by the appropriate factor, prior to time delay estimation.<sup>12,13</sup> This preprocessing has been shown to significantly improve the correlation between the pre- and postcompression signals and it compensates fairly well for the effect of compression at low strains. However, two fundamental limits arise: first, a prior knowledge of the strain magnitude is required; second, the proper temporal stretching factor depends on the local strain and cannot be constant over the signal. It therefore seems more accurate to estimate strain directly from the estimation of local scaling factors. A first study was carried out by Alam et al,<sup>14</sup> which showed that using local scaling factors leads to a method that is much more robust in terms of decorrelation noise.

In this paper, we present a method whose adaptability makes it very appropriate for the computation of local scaling factors resulting from larger strains or a wide spread of strain variations. It is expected that this method will increase the range of accurate strain measurements. To achieve maximum accuracy, the method first adaptively selects corresponding segments in the pre- and postcompression echo signals. It is essential to work with two signal segments that are representatives of the same part of tissue. The scaling factor is then estimated by iterative variation until reaching the zero of the phase of the complex cross-correlation function of the corresponding base-band signals. This is, in practice, performed by dichotomy.

The theoretical framework of our paper is described in section 2 followed by a discussion of the method's implementation in section 3. Finally, results from simulations and experimental data from a sponge phantom and a three-layer tissue-mimicking phantom are presented in section 4.

## 2. THEORY

### A. Biological tissue modeling

Modeling a soft biological tissue for elastography purposes must take mechanical as well as acoustical properties into account. Acoustically, tissue can be considered as a discrete medium of randomly distributed acoustical scatterers. It can thus be modeled as a sum of Dirac distributions weighted by the scattering strength  $A_k$  as follows

$$m_1(t) = \sum_k A_k \delta(t - t_k) \quad (1)$$

where  $t_k$  is the time of flight corresponding to the location of the  $k^{\text{th}}$  scatterer.

Mechanically, a soft biological tissue can be modeled as a continuous, isotropic, and incompressible medium composed of regions of different Young's moduli. These regions can be of variable shape, size and location.

## B. Deformation law analysis

The constitutive law of a medium depends on several intrinsic parameters such as the Young's moduli, geometry, etc. and increases in complexity with the complexity of the nature and structure of the medium. In the general case, the strain tensor  $\epsilon$  is given by

$$\epsilon = \begin{bmatrix} \epsilon_{xx} & \epsilon_{xy} & \epsilon_{xz} \\ \epsilon_{xy} & \epsilon_{yy} & \epsilon_{yz} \\ \epsilon_{xz} & \epsilon_{yz} & \epsilon_{zz} \end{bmatrix} \quad (2)$$

where  $\epsilon_{xx}$ ,  $\epsilon_{yy}$ ,  $\epsilon_{zz}$  represent elongation and  $\epsilon_{xy}$ ,  $\epsilon_{xz}$ ,  $\epsilon_{yz}$  distortion. The  $x$ ,  $y$ , and  $z$  axes correspond to the axial, lateral and elevational directions, respectively.

Under the conditions of uniaxial loading and low friction (ideally null), the stress field is uniform and monodimensional. These conditions can be approximated when the compression is performed with a plate that is larger than the medium under investigation<sup>15,16</sup> and when gel is used between the plate and the tissue to minimize friction. In such a case, the strain tensor is rewritten in Eq. (3), which clearly shows that the medium will undergo a 3-D motion, where the lateral and elevational strains are directly proportional to the axial strain. Therefore, those strains could be estimated directly from the axial strain, by multiplication by a factor  $\nu$ , which is the Poisson's ratio, nearly equal to 0.5 for biological tissues.

For those reasons, we focus on the estimation of the axial component of the strain tensor.

$$\epsilon = \begin{bmatrix} \epsilon_{xx} & 0 & 0 \\ 0 & -\nu\epsilon_{xx} & 0 \\ 0 & 0 & -\nu\epsilon_{xx} \end{bmatrix} = \begin{bmatrix} \sigma/E & 0 & 0 \\ 0 & -\nu\sigma/E & 0 \\ 0 & 0 & -\nu\sigma/E \end{bmatrix} \quad (3)$$

In this section, we will consider layered media submitted to a uniaxial loading in the  $x$  direction. Under the external stress  $\sigma$ , each layer will be deformed,<sup>17</sup> verifying the physical laws

$$E_i = \frac{\sigma}{\epsilon_i} \quad (4)$$

$$\epsilon_i = \frac{\Delta L_i}{L_i} \quad (5)$$

where  $E_i$  is the Young's moduli of the  $i^{\text{th}}$  layer,  $L_i$  its initial length,  $\Delta L_i$  the difference in length between the rest and compressed states and  $\epsilon_i$  the strain induced by the stress  $\sigma$ . Therefore,

any scatterer initially located in the  $k^{\text{th}}$  layer at the position  $l_{k0}$ , will be, after compression, at the location  $l_k$  so that

$$l_k = \sum_{i=1}^{k-1} (1 - \varepsilon_i) L_i + (1 - \varepsilon_k) l_{k0} = \sum_{i=1}^{k-1} \alpha_i L_i + \alpha_k l_{k0} \quad (6)$$

with

$$\varepsilon_i = 1 - \alpha_i \quad (7)$$

The first term in Eq. (6) corresponds to the deformation of the upper layers and can also be interpreted as the new location of the layer  $k$  within the tissue. The second term corresponds to the deformation within the layer  $k$  itself. Eq. (6) clearly shows that the tissue motion and therefore the deformation can be seen as the application of a succession of local scaling factors  $\alpha_k$ . In each layer,  $\alpha_k$  is a constant. This is the parameter we wish to estimate from rf ultrasound signals.

### C. Computing the local scaling factor

In this section, we will develop a method adapted to computing a scaling factor from two rf echo signals,  $s_1$  and  $s_2$ . It is assumed that this factor is constant over the window of study, i.e., that the postcompression signal is an exact scaled replica of the precompression signal. The scaling factor is denoted by  $\alpha$ . For our application,  $\alpha$  is a compression factor resulting from the deformation of the medium.

$$s_2(t) = s_1(\alpha t) = s_1(t + (\alpha - 1)t) = s_1(t + \tau(t)) \quad (8)$$

From Eq. (8), we can interpret the scaling factor as a variable delay, a function of the position within the window of study. Therefore, it cannot be directly computed with cross-correlation. However, if we stretch the postcompression echo signal, it will be increasingly correlated with the precompression echo signal as the stretching factor compensates for the compression. The conventional normalized autocorrelation function has a maximum equal to 1 at zero lag, which also meets the zero of the phase of the complex correlation function of corresponding analytic signals. Since the variable delay, induced by the scaling factor, is directly related to the phase of signals, it seems adequate to use the phase information.

The expression of the complex cross-correlation function is given by

$$\langle \tilde{s}_1, \tilde{s}_2 \rangle(\tau) = \frac{1}{T} \int_0^T \tilde{s}_1(t) \tilde{s}_2^*(t + \tau) dt \quad (9)$$

with  $\tilde{s}_1$  (respectively  $\tilde{s}_2$ ), the analytic signal associated to the rf echo signal  $s_1$ . We defined the function  $\varphi$  so that

$$\varphi(\beta) = \arg\left(\frac{1}{T} \int_0^T \tilde{s}_1(t) \tilde{s}_2^*(\beta t) dt\right) \quad (10)$$

The phase  $\varphi$  of the complex cross-correlation function of  $s_1$  and a stretched version of  $s_2$  is calculated at zero lag as a function of the scaling factor  $\beta$ . Indeed, we have assumed that  $s_2$  is a pure scaled replica of  $s_1$ , not suffering from any delay.

The phase  $\varphi$  is a continuous linear and strictly monotonic function. We can observe that, when  $\varphi$  is positive,  $s_2$  is a stretched version of  $s_1$ , when it is zero,  $s_2$  is identical to  $s_1$  and when  $\varphi$  is negative,  $s_2$  is a compressed version of  $s_1$ . It is interesting to note that  $\varphi$ , for a given value of  $\beta$ , represents also the phase of an averaged value, which is the scalar product averaged on the time interval  $T$ . This leads to a reduction of phase fluctuations in the presence of additive noise.

Consequently, from a practical point of view, the local scaling factors are evaluated by iteratively stretching the post-compression echo signal until reaching the zero of the phase of the complex cross-correlation function.<sup>11</sup> Finding the zero crossing is achieved by dichotomy. This technique consists of performing a framing of a zero of a function and reducing this framing until reaching the searched value with the desired accuracy. First, an interval containing the zero of the phase function is given as initial condition. The sign of the phase therefore changes on this interval. Then, the interval is iteratively reduced by keeping a sign change. This method offers the advantage of being accurate and of rapidly converging to the solution. It is interesting to note that, since the unwrapped phase is a monotonic function, it is very well adapted to such processing. The estimated stretching factor  $\hat{\beta}$  is the inverse value of the compression factor of the medium,  $\alpha$ .

$$\hat{\beta} \text{ so that } \varphi(\hat{\beta}) = 0 \text{ with } \varphi(\beta) = \arg\left(\frac{1}{T} \int_0^T \tilde{s}_1(t) \tilde{s}_2^*(\beta t) dt\right) \quad (11)$$

### 3. IMPLEMENTATION

The implementation of our processing requires three main steps:

- (1) adaptive windowing
- (2) strain estimation
- (3) a feedback loop.

#### A. Adaptive windowing

When performing adaptive windowing, corresponding segments are truncated from the pre- and postcompression echo signals. To achieve a maximum of correlation between the two signals and therefore to estimate the scaling factor with a maximum of accuracy, it is essential to work with two signal segments that are representatives of the same part of tissue. This adaptive windowing is based on the principle that while regularly displacing the window of study on the precompression signal,<sup>12</sup> this window is adaptively displaced on the signal after compression. The window displacement is a function of the previous strain estimates.<sup>13</sup>

$$d_i = i\Delta \quad (12)$$

$$d'_i = d'_{i-1} + (1 - \varepsilon_{i-1})\Delta = \sum_{k=0}^{i-1} (1 - \varepsilon_k)\Delta \quad (13)$$

where  $d_i$  is the window displacement on the precompression signal,  $d'_i$  is the window displacement on the postcompression signal and  $\Delta$  is the window displacement step.

Eq. (14) clearly shows that the displacement is adapted at each step. The more the tissue is compressed, the less displacement there will be. So, for no tissue deformation ( $\epsilon = 0$ ), the window displacement on the pre- and postcompression signal is identical and therefore the relative window displacement between the pre- and postcompressed states will be zero. Otherwise, the higher the strain the more this relative displacement will increase.

## B. Strain estimation

Having selected two corresponding signal segments, the second step of our method is the estimation of the scaling factor itself. This estimation is performed iteratively, using an algorithm of dichotomy. The postcompression signal is first stretched by a factor  $\beta$ . Then, the phase is computed and the stretching factor is varied until reaching the zero crossing of that function.

Since we are working with sampled data, precisely estimating the local scaling factor will require interpolation. So, for practical reasons, we will use baseband signals for the estimation of the phase, given that the root of the complex correlation of analytic or base-band signals is the same. Linear interpolation can be used with baseband signals, which is both accurate and fast.<sup>11</sup> Baseband signals are computed from the analytic form as follows

$$s_{lb}(t) = \tilde{s}_1(t)e^{-j\omega_0 t} \quad (14)$$

The strain estimate is finally computed as

$$\epsilon = 1 - \frac{1}{\hat{\beta}} \quad (15)$$

## C. Feedback loop

The expression given by Eq. (13) is exact when the postcompression signal is a pure scaled replica of the precompression signal and when strains are correctly estimated. However, in practice, the postcompression signal is a distorted scaled replica of the precompression signal. It is subjected to a variation of the scaling factor over the window of study, leading to an erroneous strain estimation. For these reasons, it is sometimes necessary to readjust the temporal window position.<sup>16</sup> We denote  $d'_{ic}$  the corrected window displacement, and  $\delta$  the corrective term, a term of small magnitude compared to  $d'_{ic}$ .

$$d'_{ic} = d'_i + \delta \quad (16)$$

with

$$\delta \text{ so that } c(\delta) = \max(c(t)) \quad \text{with} \quad c(t) = \int s_1(\tau)s_2(\hat{\beta}(t + \tau))d\tau \quad (17)$$

$\delta$  is computed as the location of the cross-correlation function maximum between the pre-compression signal and the postcompression signal, stretched by the estimated scaling factor. Then the scaling factor  $\beta$  is iteratively estimated once again. The process is reiterated until reaching  $\delta = 0$ .

The feedback loop permits readjustment of the adaptive windowing, in case it has performed badly due to an erroneous strain estimation.

## 4. RESULTS

To evaluate the performance of the implemented method, we tested our algorithm on simulations and experimental data.

### A. Simulations

We first studied the case of a three-layer medium subjected to a low compression. The simulated mechanical body consisted of a region  $36 \times 15 \text{ mm}^2$ , composed of three distinct 12 mm homogeneous layers. The Young's moduli of the middle layer was assumed to be twice as low as that of the other two. This medium was simulated as a set of scatterers with uniformly distributed locations, and possessing strengths that were normally distributed within the range  $[-1, 1]$ . FIELD software was used to construct rf ultrasound A-lines<sup>18</sup> using the following parameters. The pulse of 7.5 MHz center frequency is a sine function weighted by a Gaussian function of a 60 % fractional bandwidth at  $-6 \text{ dB}$ . A high 360 MHz sampling frequency was used in order to avoid further interpolation and additional computational errors that would not be directly related to the estimation method itself. The speed of sound was assumed to be constant, equal to 1540 m/s. A random additive noise was generated and scaled to produce a signal-to-noise ratio of 40 dB. We then simulated a low uniaxial loading of this medium, resulting in a uniform and monodimensional stress field. The low compression was assumed to induce a constant strain of 1%, 2%, and 1% in the layers. The different strain levels were created by decreasing the spacing between scatterers in a corresponding proportion.

Finally, elastograms were computed by estimating the local scaling factors between each congruent pair of rf A-lines, as indicated above. A correlation kernel of 1 mm (approximately 5 wavelengths) was used with 60% overlap. A median filtering was applied to these estimates to reduce noise.

In order to evaluate the accuracy of our method, we computed the average strain profile for the elastogram, including its standard deviation, and compared it with the theoretical profile. Figure 1(a) shows that the mean values of the estimates are close to the theoretical values. More precisely, for the region of 1% theoretical deformation, the mean strain was estimated at 0.97% and for the region of 2% induced strain, it was estimated at 1.95%. The standard deviation is higher for the region of 2% strain than for the region of 1% strain, but remains low over the profile. For the regions of strain discontinuity, the estimation appears less accurate (see the borders of each region, figure 1(a)). This can be easily explained. First, the studied strain profile is an extreme case since it presents vertical edges (infinite slopes). This means that the strain will vary instantaneously by one or several magnitudes, with no transition. This represents the most difficult case possible, explaining the decrease in accuracy for such regions. Our method then assumes a constant strain for the window of study. This assumption is clearly not verified when this window is positioned on a region of strain discontinuity. The estimate will be much more an averaged value of the strains of the two layers, leading to an increasing estimation error. However, this decrease in accuracy is very local and does not influence the following estimations.

The results being satisfactory for small strains, we then studied the medium previously described but subjected to a higher compression. The induced strains were assumed to be 3%, 6%, and 3%, respectively. The results illustrated in figure 1(b) show that although the deformation is much greater, our method still gives a good estimation of strains, with a low standard deviation. The mean strain for the region of 3% theoretical strain is estimated at 2.98% and at 5.9% for the region of 6% induced strain. Strain estimates remain in good agreement with the expected values. The standard deviation increases with strain, but it remains low for

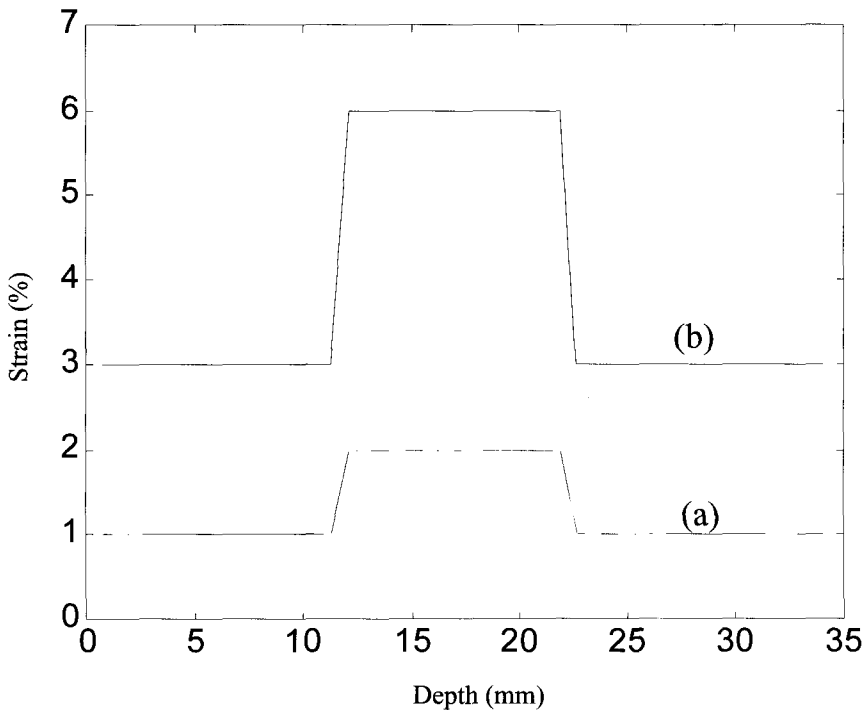


**FIG. 1** Average strain profile and standard deviation computed with a study window length of 1 mm with 60% overlap, for a three-layer medium submitted to (a) low deformation: 1%, 2%, 1% (b) higher deformation: 3%, 6%, 3%. In each case, strain estimates are very close to the theoretical profile (solid line). Standard deviation increases with strain but remains low for each profile.

the profile. Furthermore, as in the previous case, the estimation is less accurate where the strain profile ruptures, but this has no consequence on the following estimations.

Finally, to show the necessity of an adaptive displacement of the window of study, we computed the relative displacement between the pre- and postcompression signals. Results are presented in figure 2, which illustrates the change and the magnitude of this window displacement in terms of depth for the two previously studied cases. By definition, the slope of these curves will correspond to the strain estimation. As expected, the higher the strain the greater the relative displacement. Each curve is composed of three distinct segments with slopes equal to 1%, 2%, and 1% in the first case and 3%, 6%, and 3% in the second one. These values are in agreement with the amplitude of the simulated deformation and the previous strain estimates. Note that this method is sensitive to the rupture of the slope and therefore to the location of the regions of strain discontinuities. But the most fundamental observation remains that the relative displacement for the higher strain at the end of the signals is up to 1.2 mm, greater than the length of the window of study. This means that without this adaptive displacement, we would have processed two totally decorrelated signals. Consequently, adaptive displacement of the window of study is essential for an accurate estimation of the deformation.

In order to measure the range of reliability of this estimation, we computed the mean estimated strain and standard deviation as a function of the true strain (Fig. 3). Results show an accurate estimation of the mean strain with low standard deviation for strains up to 7%. At higher strains, the accuracy of the method decreases. For very low strains (0.25% - 0.5%), the standard deviation is higher than for 1% strain, but it remains acceptable. Indeed, very

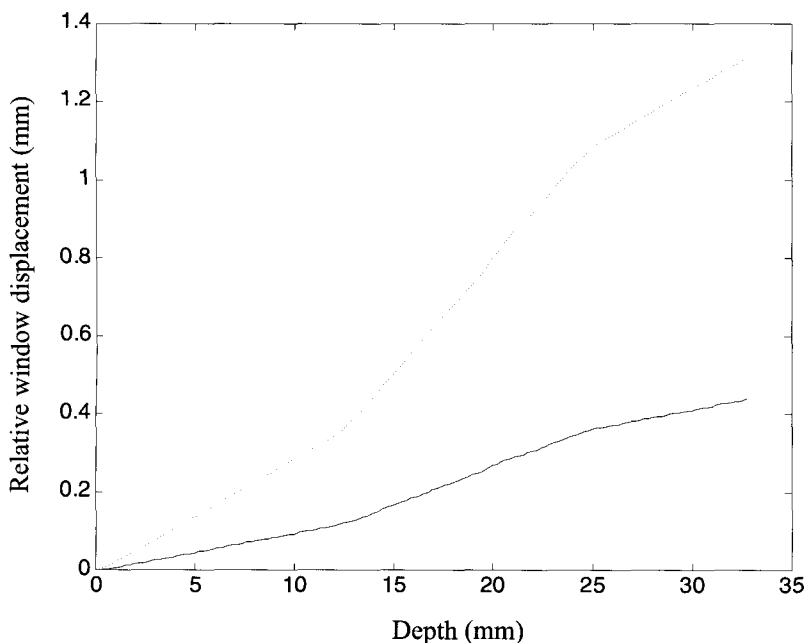


**FIG. 2** Relative displacement of the window of study between the pre- and postcompression signals computed in the case of the three-layer medium subjected to low strain (1%, 2%, 1%; solid line) and high strain (3%, 6%, 3%; dashed line).

low strains result in a very slight variation in signal shape that is hardly perceptible. This complicates the estimation.

For strains up to 7% however, our results showed that the proposed method was accurate and robust in terms of the decorrelation noise, increasing the range of precise strain estimation.

## B. Experiments

We tested our algorithm on experimental data from two phantoms. The first evaluation was performed on a set of experimental data from a sponge phantom containing a spherical hard inclusion. This inclusion, consisting of agar-agar, had a diameter of approximately 1.5 cm. In particular, it has no different acoustical properties compared to the background (Fig. 4(a)). A data-capture system for elasticity imaging was built allowing both the induction of a controlled deformation and data acquisition: a clinical ultrasound scanner and a plate were adapted on a vertical positioning slider of a controlled step compressor device. The plate was used to increase the area of loading and approximate the conditions of uniaxial loading. Accurate displacements and strains were therefore induced at the top of the phantom by vertically lowering the transducer. All displacements were measured from the face of the transducer. Data were acquired with an ultrasound probe with 7.2 MHz center frequency with 60% fractional bandwidth at  $-6$  dB. The sampling frequency was 36 MHz.

The phantom was placed in a water tank and the ultrasound transducer was initially preloaded to insure proper contact. Then, an average deformation of 1% was induced. Rf images composed of 312 lines of 1,920 samples were stored on disk and processed off-line. A preliminary resampling of the data was performed by an exact interpolation of 10:1. Then the elastogram was computed by estimating the local scaling factors, between each pair of congruent rf A-lines. The parameters were set as the same value as those chosen for strain es-

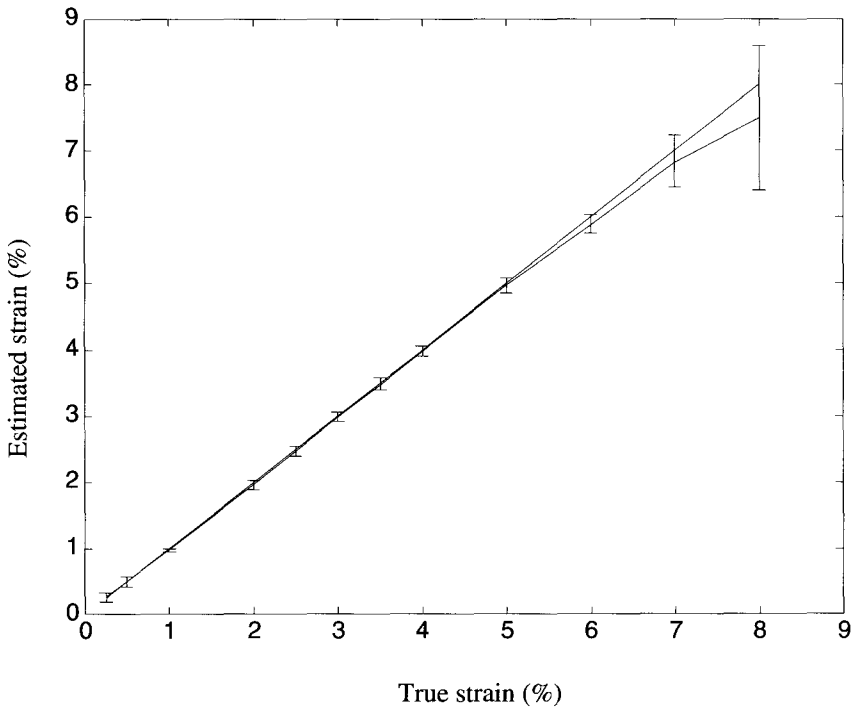


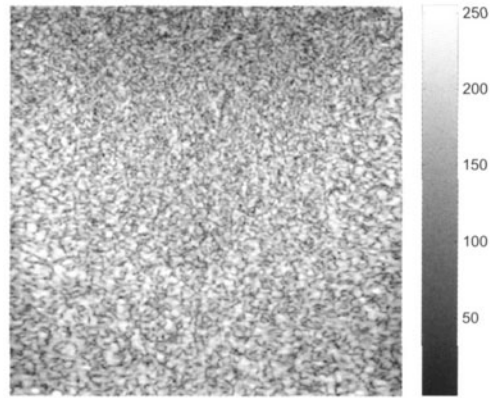
**FIG. 3** Estimated mean strain and standard deviation as a function of the true strain. The method is reliable for strains up to 7%.

timation with the simulated data. A correlation kernel of 1 mm (approximately 5 wavelengths) was used with an overlap of 60%. The elastogram is displayed in figure 4(b) with a linear gray-scale in which black corresponds to 0% strain (hard region) and white to 6.8% strain (soft region). A 5 x 5 median filtering was applied on the resulting elastogram to reduce noise (Fig. 4(c)).

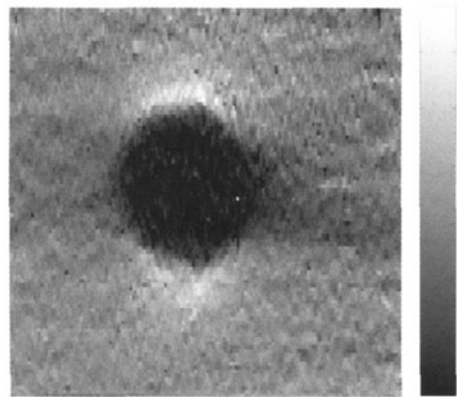
Figures 4(b) and (c) show that our algorithm distinguishes the different elastic properties of a medium. Indeed, although the hard inclusion was not visible on a classical B-scan image, it was clearly brought out on the elastogram. Moreover, the boundaries of the hard inclusion were well defined, which confirms the sensitivity of this method to the strain discontinuities and its adaptability in the processing of a medium submitted to a large spread of strain variations.

The method was also tested on a set of experimental data from a gel-based phantom. A three-layer tissue mimicking phantom was made from a solution of agar and gelatin. The top and the bottom layers have the same stiffness and the middle one is softer. At a fixed concentration of gelatin, gels with different hardness can be obtained by varying the agar concentration. Hard layers were made from a solution of 6% (by weight) gelatin and 4.5% agar, and the soft one was made using 6% gelatin and 1% agar. In each solution, we added 1% carborundum particles (Silicon-Carbide (SiC), ranging from 15  $\mu\text{m}$ ) for scattering. Attention was taken for building an acoustical homogeneous phantom with no bright internal interfaces.

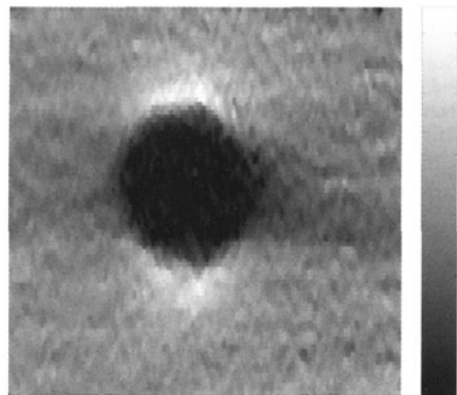
The elastogram was computed using a correlation kernel of 1 mm with 60% overlap. Results are presented in figure 5. In figure 5(a) is displayed the conventional B-mode image, where the three layers are not distinguishable. However these three layers are clearly detected on the resulting elastogram (Fig. 5(b)) with well-defined internal boundaries.



(a)

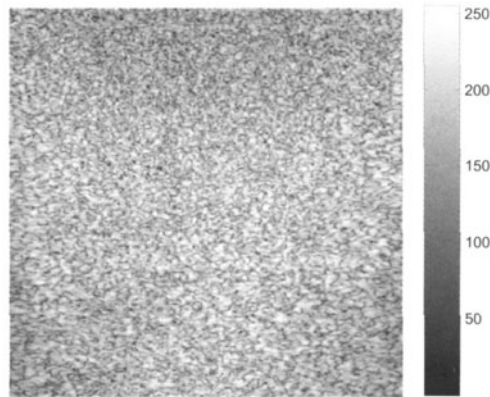


(b)

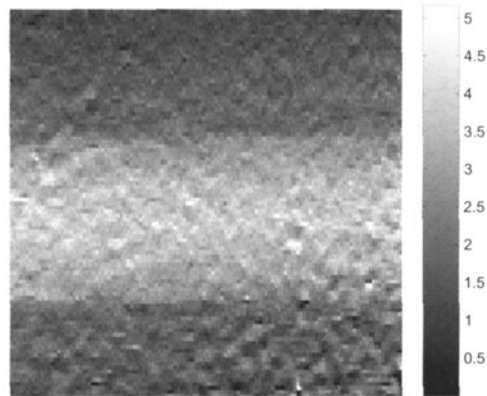


(c)

**FIG. 4** (a) Classical B-scan image of the ROI (4 cm x 4 cm), displayed with a logarithmic gray scale. The hard inclusion is not visible. (b) Corresponding elastogram of the 4 x 4 cm ROI in linear gray scale where black corresponds to 0% strain (hard region) and white to 6.8% strain (soft region). The 1.5-cm diameter agar-agar inclusion is clearly detected. (c) Elastogram of the 4 x 4 cm ROI after 5 x 5 median filtering, displayed in linear gray scale where black corresponds to 0% strain and white to 6.3% strain.



(a)



(b)

**FIG. 5** (a) Classical B-Scan image of the ROI (4 cm x 4 cm), displayed with a logarithmic gray scale. The three layers are not distinguishable. (b) Corresponding elastogram of the 4 x 4 cm ROI in linear gray scale where black corresponds to 0% strain (hard region) and white to 5% strain (soft region). The three layers are clearly detected with well defined internal boundaries.

## 5. CONCLUSIONS

We have developed a signal-processing technique to map the strain distribution occurring in a medium exposed to mechanical compression. This method is based on an adaptive and iterative estimation of local scaling factors. Results show how this method can track various local deformations in a medium. The estimation of strains gives a high level of accuracy for strains up to 7% with low standard deviations. Results for regions of strain discontinuity are less accurate, but this is very local and mainly due to the fact that the studied profiles correspond to extreme cases where variations of strains present infinite slopes. A first evaluation with experimental data has shown how such an algorithm can separate regions of different Young's moduli and has shown its potential for the detection of hard inclusions. For those reasons, we can expect that the adaptive method is suitable for mapping the elastic properties

of biological tissues with a wide spread of strain variations. Our future research efforts will concentrate on this experimental aspect of elastography.

## ACKNOWLEDGMENTS

This work was supported by the French and German Governments (PROCOPE project).

The authors also would like to thank Mr. W. Wilkening from the Department of Electrical Engineering and Information Technology, Ruhr University, Bochum, Germany for his participation during rf data acquisitions.

## REFERENCES

1. Ophir, J., Céspedes, I., Ponnekanti, H., Yazdi, Y. and Li, X., Elastography: a quantitative method for imaging the elasticity of biological tissues, *Ultrasonic Imaging* 13, 111-134 (1991).
2. Hearn, E.J., *Mechanics of Materials: An Introduction to the Mechanics of Elastic and Plastic Deformation of Solids and Structural Materials*. Third Edition (Heinemann, London, 1997).
3. Céspedes, I., Elastography: Imaging Biological Tissue Elasticity, Ph.D Dissertation, (Department of Electrical Engineering, Faculty of Houston, 1993).
4. De Korte, C.L., Van der Steen, A.F.W., Dijkman, B.H.J. and Lancee, C.T., Performance of time delay estimation methods for small time shifts in ultrasonic signals. *Ultrasonics* 35, 263-274 (1997).
5. Céspedes, I. and Ophir, J., Reduction of image noise in elastography. *Ultrasonic Imaging* 15, 89-102 (1993).
6. Hein, A. and O'Brien, W.J., Current time-domain methods for assessing tissue motion by analysis from reflected ultrasound echoes - a review. *IEEE Trans. Ultrason. Ferroelec. Freq. Contr.* 40, 84-102 (1993).
7. Konofagou, E.E., Alam, S.K., Ophir, J. and Krouskop, T., Methods for dynamic range expansion and enhancement of the signal-to-noise ratio in elastography, in *IEEE Ultrasonics Symposium*, 1157-1160 (Toronto, 1997).
8. Lubinski, M.A., Emelianov, S.Y. and O'Donnell, M., Speckle tracking methods for ultrasonic elasticity imaging using short-time correlation. *IEEE Trans. Ultrason. Ferroelec. Freq. Contr.* 46, 82-96 (1999).
9. O'Donnell, M., Skovoroda, A.R., Shapo, B.M. and Emelianov, S.Y., Internal displacement and strain imaging using ultrasonic speckle tracking. *IEEE Trans. Ultrason. Ferroelec. Freq. Contr.* 41, 314-324 (1994).
10. Konofagou, E. and Ophir, J., A new elastographic method for estimation and imaging of lateral displacements, lateral strains, corrected axial strains and Poisson's ratio in tissues. *Ultrasound Med. Biol.* 24, 1183-1199 (1998).
11. Pesavento, A. et al, A time-efficient and accurate strain estimation concept for ultrasonic elastography using iterative phase zero estimation. *IEEE Trans. Ultrason. Ferroelec. Freq. Contr.* 46, 1057-1067 (1999).
12. Kaiser Alam, S. and Ophir, J., Reduction of signal decorrelation from mechanical compression of tissues by temporal stretching: applications to elastography. *Ultrasound Med. Biol.* 23, 95-105 (1997).
13. Chaturvedi, P., Insana, M.F. and Hall, T.J., Testing the limitations of 2-D companding for strain imaging using phantoms. *IEEE Trans. Ultrason. Ferroelec. Freq. Contr.* 45, 1022-1031 (1998).
14. Alam, S.K., Ophir, J. and Konofagou, E., An adaptive strain estimator for elastography. *IEEE Trans. Ultrason. Ferroelec. Freq. Contr.* 45, 461-472 (1998).
15. Bilgen, M. and Insana, M.F., Deformation models and correlation analysis in elastography. *J. Acoust. Soc. Am.* 99, 3212-3224 (1996).
16. Ponnekanti, H., Ophir, J. and Céspedes, I., Axial stress distributions between coaxial compressors in elastography: an analytical model. *Ultrasound Med. Biol.* 18, 667-673 (1992).
17. Kurz, W., Mercier, J.P. and Zambelli, G., *Traité des Matériaux*. (Presses Polytechniques, Lausanne, 1989).
18. Jensen, J.A. and Svendsen, N.B., Calculation of pressure fields from arbitrarily shaped, apodized, and excited ultrasound transducers. *IEEE Trans. Ultrason. Ferroelec. Freq. Contr.* 39, 262-267 (1992).